International Journal For Advanced Research In Science & Technology
A peer reviewed international journal
www.ijarst.in
ISSN: 2457-0362

POWER FACTOR CORRECTION IN SRM MOTOR DRIVES USING BOOST CONVERTERIN CONTINUOUS CONDUCTION MODE

Botcha Ganesh
M-tech Student Scholar
Department of Electrical & Electronics Engineering,
Sarada Institute of Science Technology & Management;
Srikakulam(Dt),A.P, India.

S. Deep Santosh
Assistant Professor
Department of Electrical & Electronics Engineering,
Sarada Institute of Science Technology & Management;
Srikakulam(Dt),A.P, India.

Abstract—In this paper, leads to a more accurate analysis than the traditional modelling developed for dc–dc converters, which is often extended to rectifiers. It consists of a fast and concise solution for the implementation of several PFC techniques from the derived transfer functions. The introduced method is described aiming at the development of a boost-based PFC stage using the well-known one-cycle control technique (OCC) at AC mains in switched reluctance motor (SRM) drive. Aiming at low power household applications, SRM is demonstrated as one of the fine selection because of its simple construction and winding free rotor. The speed of SRM is controlled by varying the DC-bus voltage appearing across the Proposed converter of SRM. The proposed converter working in discontinuous inductor current mode is used to regulate the DC output voltage and improves the power quality at the AC mains. Simulation results are presented in Mat Lab SimuLink Software.

Key words: switched reluctance motor (SRM), one-cycle control technique (OCC), PFC

I. INTRODUCTION

The electrical drives play a crucial role to any industrial and commercial applications. Switched reluctance motor has become an alternative to permanent magnet brushless motors and other relative motor in many industrial applications. The disadvantage of switched reluctance motor is acoustic ripple, high torque ripple, and difficult to control. Switched reluctance motor has gain its attention because of increase in power electronic devices. Switched reluctance motors are mechanically and electrically more rough than conventional AC and D.C motors. Discrete production nature of torque mechanism in SRM causes torque pulsation is non-linear. The Work of air conditioner is to maintain the surrounding air temperature equal to the set reference continuously. The improved efficiency of the compressor in air conditioning system achieved only by controlling the speed of the drive for maintaining optimal temperature of the surroundings. Air conditioning system with switched reluctance motor has ruggedness inexpensive manufacturing capability and long life. Switched reluctance motor speed can be varied by varying the D.C link voltage to the voltage which is proportional to the rpm of the motor.

Switches of bridge converter (asymmetric) is turned on or off based on rotor position which is sensed by rotor position sensor of SRM and hysteresis current control technique. Charging of D.C link capacitor which is almost uncontrolled causes a high peak in ac input current. Uncontrolled charging of capacitor results in power quality problems in terms of power factor (PF) which is less, high total harmonic distortion (THD) and crest factor (CF). In this paper proposed, voltage control drive is Cuk D.C-D.C converter. In voltage controlled drive, PFC converter requires continuous input current, continuous output current and small output capacitive and inductive filter wide range of output voltage. Cuk converter fulfills all the requirements of the PFC converter. Proposed topology can also be used for smooth D.C link voltage control to get required speed of air conditioning.

International Journal For Advanced Research In Science & Technology
A peer reviewed international journal
www.ijarst.in
ISSN: 2457-0362

2 BRIEF ANALYSIS OF THE PFC BOOST CONVERTER IN CCM

The simplest solution for the implementation of a generalpurpose switched-mode power supply SMPS relies on singlestage converters, since they can provide high input power factor, output voltage control, low component count, and reduced low-frequency ripple, although they generally require the use of high dc-link filter capacitances [21]. Besides, a high-voltage dc link can be employed depending on the application, while the low-frequency filtering capacitance will be significantly reduced in this case, which may enable the use of long-life film capacitors. The ac–dc single-stage boost converter in CCM is perhaps the most popular solution for overall PFC applications rated at a few hundred watts owing to inherent simplicity, reduced number of power stage elements, and the continuous nature of the input current. Besides, it leads to reduced current stresses on the semiconductors, which are proportional to the input current. The conventional ac–dc boost configuration is presented in Figure 1, where PFC can be achieved using distinct control techniques. Even though ACMC is the most popular approach owing to the wide availability of dedicated commercial ICs, the control system implementation aggregates increased complexity and higher component count [7]. Indirect techniques such as the OCC are capable of overcoming such drawbacks, since they do not require multipliers, dividers, and a sample of the rectified input voltage [8]. IR1150 is the only commercial IC dedicated to OCC and will be used in this work as described in the forthcoming sections [22].

The expressions for calculating the filter elements of the acdc boost converter, i.e. Lb and Cdc are given by Equations (1) and (2), respectively

$$L_b = \frac{V_g}{f_{s(PFC)}} \cdot \frac{\overline{\Delta I_{Lb}}}{\Delta I_{Lb}} \quad (1)$$

$$C_{dc} = \frac{P_o}{2 \cdot (2\pi f_L) \cdot V_{dc} \cdot \Delta V_{dc}} \quad (2)$$

where:

$$\beta = \frac{V_{dc}}{V_g} \quad (3)$$

$$\overline{\Delta I_{Lb}} = \frac{\beta}{4} \quad (4)$$

Besides, Vg is the peak value of the input voltage; fs(PFC) is the switching frequency; ΔILb is the normalized inductor current ripple defined according to parameter β; ΔILb is the inductor current ripple at the peak grid voltage; Po is the rated output power, fL is the line frequency; Vdc is the average dc-link voltage; and ΔVdc is the dc-link voltage ripple.

The development of a simplified PFC small-signal modelling approach applied to the ac-dc boost converter will be presented in the forthcoming section. As previously mentioned, this technique considers the low-frequency dynamics associated with the ac mains and the eventual need for high dc-link capacitances used in the implementation of distinct control techniques.

3 SMALL-SIGNAL MODELLING TECHNIQUE FOR PFC CONVERTERS IN CCM

In PFC converters operating in CCM, the low-frequency component is the dominant portion in the dc-link voltage, since it influences the dynamic behaviour of the whole system directly. Therefore, the modelling methodology can be better represented in terms of an average analysis carried out for a half period of the ac grid voltage. It consists in substituting the switching elements, i.e. the active switch and diode by controlled current sources, which represent small-signal disturbances in the average currents through the semiconductors. Then, this model can be employed to analyse the influence of disturbances on the PFC converter.

First, let us consider a PFC boost converter in CCM, as some key parameters must be defined. Some typical low-frequency and high-frequency waveforms are represented in Figure 2, from which important expressions can be obtained. The rectified sinusoidal input voltage and the duty cycle, which are both time-variant, are given by Equations (5) and (6), respectively

International Journal For Advanced Research In Science & Technology
A peer reviewed international journal
www.ijarst.in
ISSN: 2457-0362

$$v_g(t) = V_g \cdot |\sin(\omega_L t)|$$

(5)

$$\frac{V_{dc}}{V_g \cdot \sin(\omega_L t)} = \frac{1}{1 - d(t)} \Rightarrow d(t) = 1 - \frac{V_g}{}$$

(6)

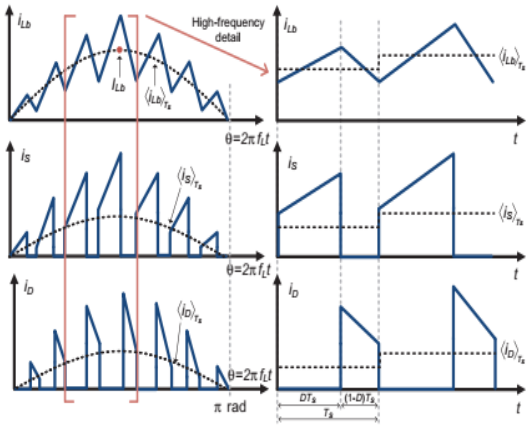

FIGURE 2 Detailed view of typical low-frequency and high-frequency waveforms of a PFC boost rectifier in CCM

where v g(t) is the instantaneous input voltage; ωL = 2·π·fL is the line angular frequency in rad/s; and d(t) is the time-variant duty cycle.

In the presented approach, the inductor current is considered constant over the switching period Ts, thus simplifying the analysis. Then, the average value of the instantaneous inductor current can be properly represented by a rectified sinusoidal waveform considering only the positive half cycle of the grid voltage.

The average values of the instantaneous inductor current and instantaneous input voltage are then described by Equation (7).

$$\langle i_{Lb} \rangle_{Ts} = I_{Lb} \cdot \sin(\theta), 0 < \theta < \pi$$
$$\langle v_g \rangle_{Ts} = V_g \cdot \sin(\theta), 0 < \theta < \pi$$

(7)

where ILb is the instantaneous average value of the peak current through the filter inductor; and θ = ωL·t is the phase angle in rad.

The currents through the active switch and diode must also be described by their respective average values over one switching period according to the high-frequency waveforms in Figure 2, resulting in:

$$\langle i_S \rangle_{Ts} = d(t) \cdot \langle i_{Lb} \rangle_{Ts}$$
$$\langle i_D \rangle_{Ts} = (1 - d(t)) \cdot \langle i_{Lb} \rangle_{Ts}$$

(8)

Substituting the duty cycle and the inductor current represented by Equations (6) and (7) in Equation (8), respectively, Equation (9) can then be obtained.

$$\langle i_S \rangle_{Ts}(t) = \left(1 - \frac{V_g \cdot \sin(\theta)}{V_{dc}}\right) \cdot (I_{Lb} \cdot \sin(\theta))$$
$$\langle i_D \rangle_{Ts}(t) = \left(\frac{V_g \cdot \sin(\theta)}{V_{dc}}\right) \cdot (I_{Lb} \cdot \sin(\theta))$$

(9)

The relationships in Equation (9) must be then integrated while considering one period of the rectified input voltage, i.e. TL/2 = 1/(2·fL), resulting in the average currents through the active switch and diode given in Equations (10) and (11), respectively. Thus, Equations (10) and (11) describe the currents in terms of both high-frequency and low-frequency components.

$$I_S = \langle \langle i_S \rangle_{Ts} \rangle_{T_L/2} = \frac{1}{\pi} \cdot \int_0^{\pi} \langle i_S \rangle_{Ts}(\theta)\, d\theta$$
$$I_S = \frac{1}{\pi} \cdot \int_0^{\pi} \left[(I_{Lb} \cdot |\sin(\theta)|) - \frac{I_{Lb} \cdot V_g}{V_{dc}} (|\sin(\theta)|)^2 \right] d\theta$$
$$I_S = I_{Lb} \cdot \left(\frac{2}{\pi} - \frac{V_g}{2 \cdot V_{dc}}\right)$$

(10)

$$I_D = \langle \langle i_D \rangle_{Ts} \rangle_{T_L/2} = \frac{1}{\pi} \cdot \int_0^{\pi} \langle i_D \rangle_{Ts}(\theta)\, d\theta$$
$$I_D = \frac{1}{\pi} \cdot \int_0^{\pi} \left[\frac{I_{Lb} \cdot V_g}{V_{dc}} (|\sin(\theta)|)^2 \right] d\theta$$
$$I_D = \frac{I_{Lb} \cdot V_g}{2 \cdot V_{dc}}$$

(11)

The average small-signal model is based on perturbing and linearizing the average circuit variables so that they can be represented in the frequency domain. Therefore, the Laplace

International Journal For Advanced Research In Science & Technology
A peer reviewed international journal
www.ijarst.in
ISSN: 2457-0362

representation for the average currents can be obtained by adding disturbances to each input parameter. Considering the active switch, the disturbance is given by Equation (12).

$$\Delta\left\langle\left\langle i_S\right\rangle_{T_s}\right\rangle_{T_L/2} = G_{Sg}\tilde{v}_g + G_{So}\tilde{v}_{dc} + G_{Si}\tilde{i}_{Lb} \quad (12)$$

where GSg, GSo, and GSi are the partial derivatives of the active switch current with respect to the input voltage, output voltage, and inductor current, respectively; v˜g, v˜dc, and ˜ıLb are the disturbances associated with the input voltage, dc-link voltage, and inductor current, respectively. The time-dependent expression can then be represented in the frequency domain as in Equation (13).

$$i_S(s) = G_{Sg}\cdot v_g(s) + G_{So}\cdot v_{dc}(s) + G_{Si}\cdot i_{Lb}(s) \quad (13)$$

where v g(s), vdc(s), and iLb(s) correspond to the input voltage, output voltage, and inductor current represented in the frequency domain, respectively. The partial derivatives of the switch current must be solved for each particular case while considering the linearized operating point. Therefore, Equations (14)–(16) result from the substitution of Equation (12) in (10).

$$G_{Sg} = \frac{\partial}{\partial V_g}\left[I_{Lb}\left(\frac{2}{\pi} - \frac{V_g}{2V_{dc}}\right)\right] = -\frac{I_{Lb}}{2V_{dc}} \quad (14)$$

$$G_{So} = \frac{\partial}{\partial V_{dc}}\left[I_{Lb}\left(\frac{2}{\pi} - \frac{V_g}{2V_{dc}}\right)\right] = \frac{I_{Lb}\cdot V_g}{2{V_{dc}}^2} \quad (15)$$

$$G_{Si} = \frac{\partial}{\partial I_{Lb}}\left[I_{Lb}\left(\frac{2}{\pi} - \frac{V_g}{2V_{dc}}\right)\right] = \frac{2}{\pi} - \frac{V_g}{2V_{dc}} \quad (16)$$

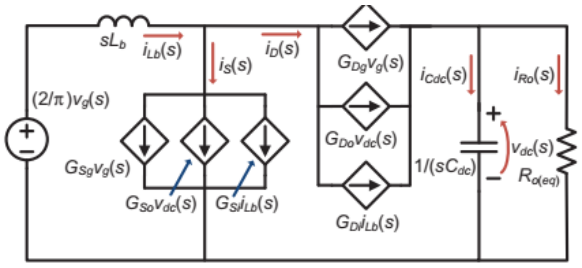

FIGURE 3 Average equivalent circuit of the PFC boost rectifier in CCM

The same analysis can be performed in the frequency domain for the passive switch, i.e. the diode according to Equation (17), resulting in Equation (18).

$$\Delta\left\langle\left\langle i_D\right\rangle_{T_s}\right\rangle_{T_L/2} = G_{Dg}\tilde{v}_g + G_{Do}\tilde{v}_{dc} + G_{Di}\tilde{i}_{Lb} \quad (17)$$

where G Dg, GDo, and GDi are the partial derivatives of the diode current with respect to the input voltage, output voltage, and inductor current, respectively.

$$i_D(s) = G_{Dg}\cdot v_g(s) + G_{Do}\cdot v_{dc}(s) + G_{Di}\cdot i_{Lb}(s) \quad (18)$$

$$G_{Dg} = \frac{\partial}{\partial V_g}\left[\frac{I_{Lb}\cdot V_g}{2V_{dc}}\right] = \frac{I_{Lb}}{2V_{dc}} \quad (19)$$

$$G_{Do} = \frac{\partial}{\partial V_{dc}}\left[\frac{I_{Lb}\cdot V_g}{2V_{dc}}\right] = -\frac{I_{Lb}\cdot V_g}{2{V_{dc}}^2} \quad (20)$$

$$G_{Di} = \frac{\partial}{\partial I_{Lb}}\left[\frac{I_{Lb}\cdot V_g}{2V_{dc}}\right] = \frac{V_g}{2V_{dc}} \quad (21)$$

The peak inductor current ILb can be calculated from the power balance applied to this element as described by Equation (22).

International Journal For Advanced Research In Science & Technology
A peer reviewed international journal
www.ijarst.in
ISSN: 2457-0362

$$\frac{I_{Lb} \cdot V_g}{2} = P_o \therefore I_{Lb} = \frac{2 \cdot P_o}{V_g} \quad (22)$$

As long as iS(s) and iD(s) are defined in the frequency domain, an equivalent average circuit can be proposed as in Figure 3, where R o(eq) is the equivalent load resistance. Thus, the average small-signal model of the PFC stage can be obtained applying Kirchhoff's circuit laws to obtain the desired transfer functions. It is well known that the series resistance of the boost inductor does not influence the dynamic response of the boost converter significantly, but only the voltage conversion ratio, while it can be neglected in the proposed modelling as suggested by [18, 19]. On the other hand, the equivalent series resistance (ESR) of the dc-link capacitor must be properly analysed depending on the construction technology. Metallized polypropylene film (MPF) capacitors present prominent advantages regarding long lifespan and extremely low ESR values when compared with their electrolytic counterparts [24]. Consequently, such parasitic element can be neglected in the desired transfer functions for particular applications that employ only long-life film capacitors in the dc link, mainly when high voltage levels exist as it was previously stated in Section 2, thus simplifying the analysis drastically. Otherwise, in applications where the use of electrolytic capacitors is inevitable, their respective ESRs should be properly incorporated to the model.

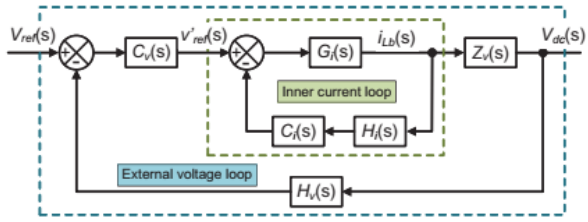

FIGURE 4 Block diagram representation of current-mode PFC techniques typically employed in high power factor rectifiers in CCM

The ratio between the output voltage and the input voltage can be determined by analysing the output node of the circuit in Figure 3 while neglecting the inductor-current-dependent portion in this case, resulting in Equation (23), which can be solved to obtain vdc(s)/vg(s) as in Equation (24). On the other hand, if the capacitor ESR should in fact be considered in a given application, this particular transfer function will be given by Equation (25), which of course can be simplified in terms of Equation (22) when the ESR is negligible.

$$G_{Dg} \cdot v_g(s) + G_{Do} \cdot v_{dc}(s) = v_{dc}(s)\left(\frac{1}{R_{o(eq)}} + sC_{dc}\right) \quad (23)$$

$$M_v(s) = \frac{v_{dc}(s)}{v_g(s)} = \frac{R_{o(eq)} \cdot G_{Dg}}{1 - R_{o(eq)} \cdot G_{Do} + s\left(R_{o(eq)} \cdot C_{dc}\right)} \quad (24)$$

$$M_{v(ESR)}(s) = \frac{v_{dc}(s)}{v_g(s)} = \frac{R_{o(eq)} \cdot G_{Dg}}{1 - R_{o(eq)} \cdot G_{Do} + \frac{s\left(R_{o(eq)} \cdot C_{dc}\right)}{s(ESR \cdot C_{dc})+1}} \quad (25)$$

A general-purpose block diagram regarding the development of current-mode control techniques is presented in Figure4, where Hi(s) and Hv(s) represent the sampling gains of the inductor current and dc-link voltage, respectively. The transfer function of the inductor current to the output voltage, i.e. Zv(s), must be determined in Figure 5 for the implementation of the control law associated with the external voltage loop. At this point, it is important to observe that this particular control loop is the one that incorporates the low-frequency dynamics of the system, while its transfer function is then required to control the output voltage accurately in a PFC rectifier.

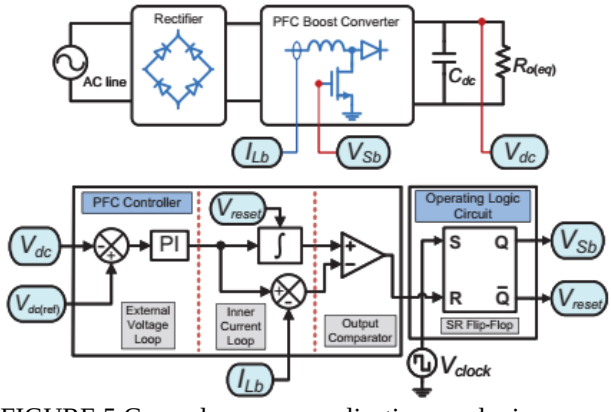

FIGURE 5 General-purpose application employing a single-stage PFC boost converter based on the OCC technique

International Journal For Advanced Research In Science & Technology
A peer reviewed international journal
www.ijarst.in
ISSN: 2457-0362

In order to obtain Z v(s), the output in Figure 3 can also be analysed while neglecting the term that depends on the input voltage. For this purpose, Equation (26) must be considered, which results in Equation (27) after some algebra. Also in this case, if the filter capacitor ESR is supposed to be considered in a particular application, such transfer function can be modified to reflect its influence as in Equation (28).

$$G_{Do} \cdot v_{dc}(s) + G_{Di} \cdot i_{Lb}(s) = v_{dc}(s)\left(\frac{1}{R_{o(eq)}} + sC_{dc}\right) \quad (26)$$

$$Z_v(s) = \frac{v_{dc}(s)}{i_{Lb}(s)} = \frac{R_{o(eq)} \cdot G_{Di}}{1 - R_{o(eq)} \cdot G_{Do} + s\left(R_{o(eq)} \cdot C_{dc}\right)} \quad (27)$$

$$Z_{v(ESR)}(s) = \frac{v_{dc}(s)}{i_{Lb}(s)} = \frac{R_{o(eq)} \cdot G_{Di}}{1 - R_{o(eq)} \cdot G_{Do} + \frac{s\left(R_{o(eq)} \cdot C_{dc}\right)}{s(ESR \cdot C_{dc})+1}} \quad (28)$$

4. Switched reluctance motor

Switched Reluctance Motors (SRM) have inherent advantages such as simple structure with non winding construction in rotor side, fail safe because of its characteristic which has a high tolerances, robustness, low cost with no permanent magnet in the structure, and possible operation in high temperatures or in intense temperature variations. The torque production in switched reluctance motor comes from the tendency of the rotor poles to align with the excited stator poles. The operation principle is based on the difference in magnetic reluctance for magnetic field lines between aligned and unaligned rotor position when a stator coil is excited, the rotor experiences a force which will pull the rotor to the aligned position. However, because SRM construction with doubly salient poles and its non-linear magnetic characteristics, the problems of acoustic noise and torque ripple are more severe than these of other traditional motors.

The torque ripple is an inherent drawback of switched reluctance motor drives. The causes of the torque ripple include the geometric structure including doubly salient motor, excitation windings concentrated around the stator poles and the working modes which are necessity of magnetic saturation in order to maximize the torque per mass ratio and pulsed magnetic field obtained by feeding successively the different stator windings. The phase current commutation is the main cause of the torque ripple.

The torque ripple can be minimized through magnetic circuit design in a motor design stage or by using torque control techniques. In contrast to rotating field machines, torque control of switched reluctance machines is not based on model reference control theory, such as field oriented control, but is achieved by setting control variables according to calculated or measured functions. By controlling the torque of the SRM, low torque ripple, noise reduction or even increasing of the efficiency can be achieved. There are many different types of control strategy from simple methods to complicated methods. In this book, motor design factors are not considered and detailed characteristics of each control method are introduced in order to give the advanced knowledge about torque control method in SRM drive.

A Construction of SRM

The Switched Reluctance Motors is an electric machine that is characterized mainly by its constructive simplicity. It has salient poles on both stator and rotor and its magnetic core consists of laminated steel. It is a doubly salient, single excited motor. Each stator pole has a simple concentrated winding and there are no conductors of any kind on the rotor which makes the construction cheaper, reliable, and rugged. The schematic diagram of an SRM with eight stator and six rotor poles is shown in Fig 4.1.The stator windings on diametrically opposite poles are connected in series to form one stator phase. The rotor is also laminated. Thinner laminations of silicon steel are preferred in SRM as eddy current dominates the core losses due to higher commutating frequency compared to AC motor of comparable speed and rating. For very high speed application, Cobalt-iron and variants are used for laminations (Miller, T.J.E (1993). The stator and rotor poles appear in pairs but are usually of unequal numbers. This is to avoid the eventuality of the rotor being in a state of producing no initial torque, which occurs when all the rotor poles are locked in with the stator poles. A unique feature of SRM is that it can be

International Journal For Advanced Research In Science & Technology
A peer reviewed international journal
www.ijarst.in
ISSN: 2457-0362

operated, even though with reduced power output, even when there is a loss of one of the phases. The choice of the number of poles and number of phases is not unique. Although the number of phases and the number of poles must be minimum to reduce the number of switching devices and the associated commutation, the torque capabilities will influence its selection. Different configurations have been studied and its influence on the performance has been reported (Miller, T.J.E (1993). In order to guarantee that the SRM can be started at any initial rotor position, and to get smooth torque capacity per resolution, SRM's with multi-phase as well as multi-rotor-pairs are developed. The number of stator and rotor poles is generally different. Some possible combinations are: $N_s = 6$, $N_r = 4$; $N_s = 8$, $N_r = 6$; $N_s = 12$, $N_r = 10$, etc. These combinations ensure that the rotor is never in a position where the summation of the electromagnetic torque generated by each phase is zero. The larger the stator and rotor poles number, the less the torque ripple. By choosing a combination where there are two more stator poles than rotor poles, high torque and low switching frequency of the power converter can be achieved. Three phase 6/4 pole and four phase 8/6 pole configurations are popular among different configurations.

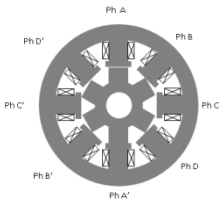

Fig 6 Cross section of a 8/6 SRM

B Characteristics of switched reluctance motor

The SRM is an electric machine that converts the reluctance torque into mechanical power. In the SRM, both the stator and rotor have a structure of salient-pole, which contributes to produce a high output torque. The torque is produced by the alignment tendency of poles. The rotor will shift to a position where reluctance is to be minimized and thus the inductance of the excited winding is maximized. The SRM has a doubly salient structure, but there are no windings or permanent magnets on the rotor [Lawrenson, 1980]. The rotor is basically a piece of steel (and laminations) shaped to form salient poles. So it is the only motor type with salient poles in both the rotor and stator. As a result of its inherent simplicity, the SRM promises a reliable and a low-cost variable-speed drive and will undoubtedly take the place of many drives now using the cage induction, PM and DC machines in the short future. The number of poles on the SRM's stator is usually unequal to the number of the rotor to avoid the possibility of the rotor being in a state where it cannot produce initial torque, which occurs when all the rotor poles are aligned with the stator poles. Fig.4.2 shows a 8/6 SRM with one phase asymmetric inverter. This 4-phase SRM has 8 stator and 6 rotor poles, each phase comprises two coils wound on opposite poles and connected in series or parallel consisting of a number of electrically separated circuit or phases. These phase windings can be excited separately or together depending on the control scheme or converter. Due to the simple motor construction, an SRM requires a simple converter and it is simple to control.

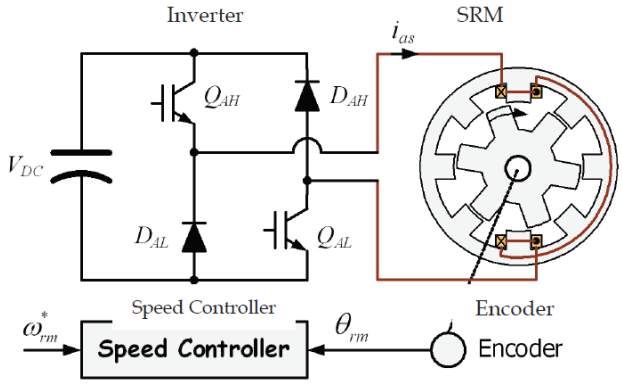

Fig. 7. SRM with one phase asymmetric inverter

The aligned position of a phase is defined to be the situation when the stator and rotor poles of the phase are perfectly aligned with each other (θ_1-θ_2), attaining the minimum reluctance position and at this position phase inductance is maximum. The phase inductance decreases gradually as the rotor poles move away from the aligned position in either direction. When the rotor poles are symmetrically misaligned with the stator poles of a phase the position is said to be the unaligned position and at this position the phase has minimum inductance . Although the concept of inductance is not valid for a highly saturated machine like SR motor, the

International Journal For Advanced Research In Science & Technology
A peer reviewed international journal
www.ijarst.in
ISSN: 2457-0362

unsaturated aligned and unaligned incremental inductances are the two key reference positions for the controller.

The relationship between inductance and torque production according to rotor position is shown in Fig. 1.3. There are some advantages of an SRM compared with the other motor type. The SRM has a low rotor inertia and high torque/inertia ratio; the winding losses only appear in the stator because there is no winding in the rotor side; SRM has rigid structure and absence of permanent magnets and rotor windings; SRM can be used in extremely high speed application and the maximum permissible rotor temperature is high, since there are no permanent magnets and rotor windings [Miller, 1988].

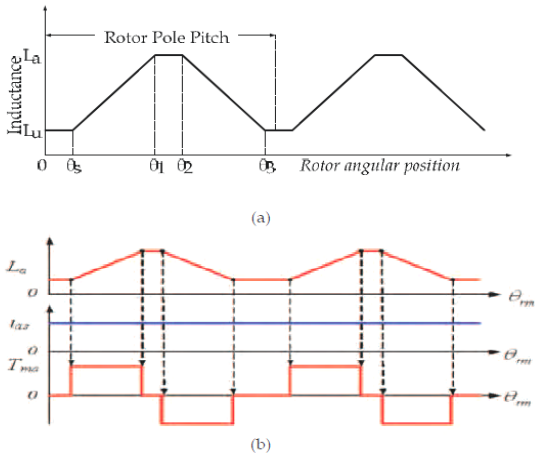

Fig. 8. (a) Inductance and (b) torque in SRM

Constructions of SRM with no magnets or windings on the rotor also bring some disadvantage in SRM. Since there is only a single excitation source and because of magnetic saturation, the power density of reluctance motor is lower than PM motor. The construction of SRM is shown in Fig. 1.3. The dependence on magnetic saturation for torque production, coupled with the effects of fringing fields, and the classical fundamental square wave excitation result in nonlinear control characteristics for the reluctance motor. The double saliency construction and the discrete nature of torque production by the independent phases lead to higher torque ripple compared with other machines. The higher torque ripple, and the need to recover some energy from the magnetic flux, also cause the ripple current in the DC supply to be quite large, necessitating a large filter capacitor. The doubly salient structure of the SRM also causes higher acoustic noise compared with other machines. The main source of acoustic noise is the radial magnetic force induced. So higher torque ripple and acoustic noise are the most critical disadvantages of the SRM.

The absence of permanent magnets imposes the burden of excitation on the stator windings and converter, which increases the converter KVA requirement. Compared with PM brushless machines, the per unit stator copper losses will be higher, reducing the efficiency and torque per ampere. However, the maximum 0speed at constant power is not limited by the fixed magnet flux as in the PM machine, and, hence, an extended constant power region of operation is possible in SRM. The torque-speed characteristics of an SRM are shown in Fig. 8. Based on different speed ranges, the motor torque generation has been divided into three different regions: constant torque, constant power and falling power region.

5.1 SIMULATION RESULTS

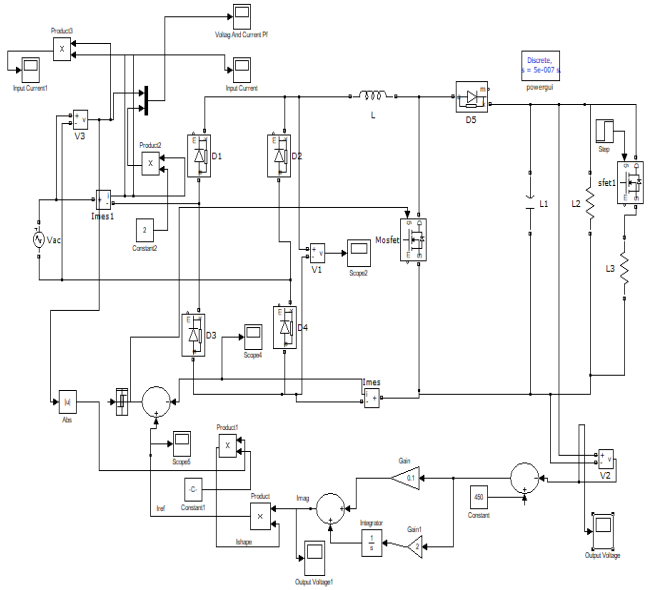

Fig 9 Simulink Diagram of Proposed DC-DC Converter with Increasing of Load

International Journal For Advanced Research In Science & Technology
A peer reviewed international journal
www.ijarst.in
ISSN: 2457-0362

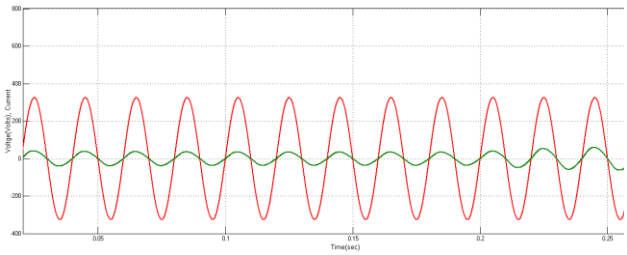

Fig 10 Simulation wave form of Proposed DC-DC Converter with Increasing of Load Input voltage & Current

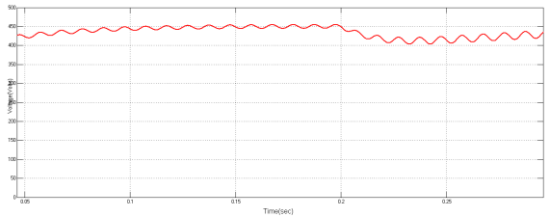

Fig 11 Simulation wave form of Proposed DC-DC Converter with Increasing of Load 0utput voltage

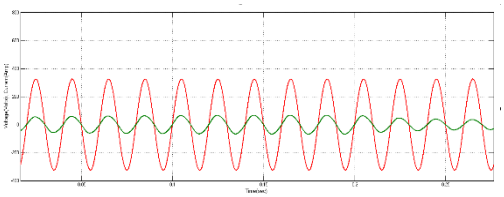

Fig 12 Simulation wave form of Proposed DC-DC Converter with Decreasing of Load Input voltage & Current

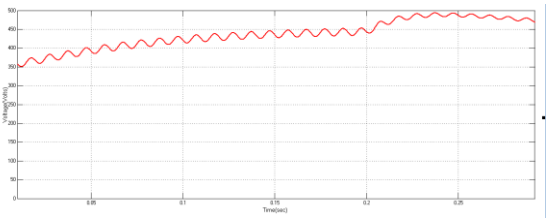

Fig 13 Simulation wave form of Proposed DC-DC Converter with Decreasing of Load output voltage & Current

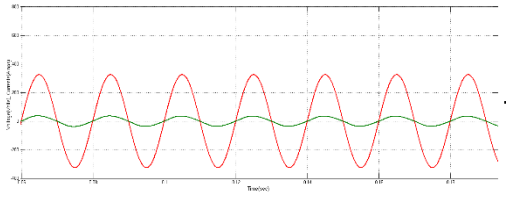

Fig 14 Simulation wave form of Proposed DC-DC Converter with Fixed of Load Input voltage & Current

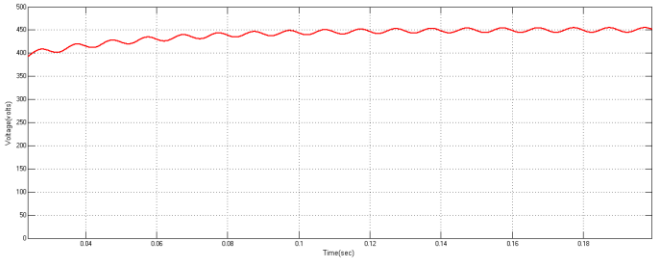

Fig 15 Simulation wave form of Proposed DC-DC Converter with Fixed of Load Ouput voltage

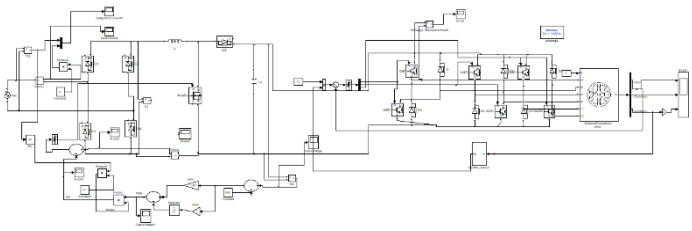

Fig 16 Simulink Diagram of Proposed DC-DC Converter with SRM Motor Drive Application

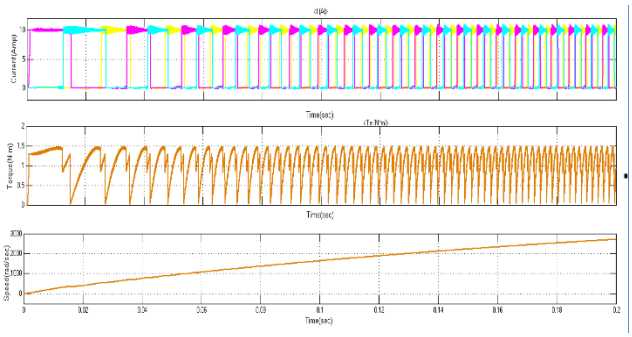

Fig 17 Simulation wave form of Proposed DC-DC Converter with SRM Motor Drive Performance of Stator current, Torque & Speed Characteristics

International Journal For Advanced Research In Science & Technology
A peer reviewed international journal
www.ijarst.in
ISSN: 2457-0362

5. CONCLUSION

A switched capacitor buck boost converter fed SRM drive has been proposed for low power applications. The design of the converter and related simulations considering performances have been performed in MATLAB/Simulink environment. This work has presented a general small-signal modelling procedure for PFC rectifiers operating in CCM. Considering that traditional techniques such as average state space and PWM switch model are not capable of reproducing the low-frequency dynamics of such converters accurately when high-value filter capacitors are used, the introduced methodology can be regarded as a simple, concise, and straightforward solution. A front-end boost rectifier was analysed in detail, whose choice is owing to the fact that this is a quite popular topology for general-purpose applications.

The small-signal model was properly validated in both time and frequency domains from relevant waveforms respectively, thus showing that it is capable of reproducing the behaviour of the PFC rectifier adequately even when highvalue filter capacitors are used. Furthermore, the closedloop control system performance related to the measured overshoot and settling time ensured the accuracy and applicability of the proposed low-frequency modelling technique, since only slight differences were verified with the simulated model.

REFERENCES

1. Nassary, M., et al.: Single-loop control scheme for electrolytic capacitorless AC–DC rectifiers with PFC in continuous conduction mode. Electron. Lett. 56(10), 506–508 (2020)
2. Qi, W., et al.: Design considerations for voltage sensorless control of a PFC single-phase rectifier without electrolytic capacitors. IEEE Trans. Indust. Electron. 67(3), 1878–1889 (2020)
3. Dong, H., et al.: A novel primary-side regulation control scheme for CCM and DCM LLC LED driver based on “magnetizing current cancellation method. IEEE Trans. Power Electron. 35(11), 12223–12237 (2020)
4. Electromagnetic compatibility (EMC) - Part 3-2: Limits - Limits for harmonic current emissions (equipment input current ≤16 A per phase). IEC 61000-3-2. International Electrotechnical Commission, Geneva (2014)
5. Electromagnetic compatibility (EMC) - Part 3-4: Limits - Limitation of emission of harmonic currents in low-voltage power supply systems for equipment with rated current greater than 16 A. IEC 61000-3-4. International Electrotechnical Commission, Geneva (2014)
6. Fischer, G.S., et al.: Extensions of leading-edge modulated one-cycle control for totem pole bridgeless rectifiers. IEEE Trans. Power Electron. 35(5), 5447–5460 (2020)
7. Rossetto, L., et al.: Control techniques for power factor correction converters. In: Proceedings of Power Electronics and Motion Control Conference (PEMC). IEEE, Piscataway, New Jersey, pp. 1310–1318 (1994)
8. Smedley, K.M., Cuk, S.: One-cycle control of switching converters. IEEE ´ Trans. Power Electron. 10(6), 625–633 (1995)
9. Borgonovo, D., et al.: A self-controlled power factor correction singlephase boost pre-regulator In: 36th Power Electronics Specialists Conference PESC’05. IEEE, Piscataway, New Jersey, pp. 2351–2357 (2005)
10. Middlebrook, R.D., Cuk, S.: A general unified approach to modelling switching-converter power stages. In: Power Electronics Specialists Conference. IEEE, Piscataway, New Jersey, pp. 18–34 (1976)
11. Cuk, S., Middlebrook, R.D.: A general unified approach to modelling switching DC-to-DC converters in discontinuous conduction mode. In: Power Electronics Specialists Conference. IEEE, Piscataway, New Jersey, pp. 36– 57 (1977)
12. Polivka, W.M., et al.: State-space average modelling of converters with parasitics and storage-time modulation. In: Power Electronics Specialists Conference. IEEE, Piscataway, New Jersey, pp. 119–143 (1980)
13. Smithson, S.C., Williamson, S.S.: A unified state-space model of constantfrequency current mode-controlled power converters in

International Journal For Advanced Research In Science & Technology
A peer reviewed international journal
www.ijarst.in
ISSN: 2457-0362

continuous conduction mode. IEEE Trans. Indust. Electron. 62(7), 4514–4524 (2015)
14. Vorperian, V.: Simplified analysis of PWM converters using model of PWM switch. Continuous conduction mode. IEEE Trans. Aerosp. Electron. Syst. 26(3), 490–496 (1990)
15. Vorperian, V.: Simplified analysis of PWM converters using model of PWM switch. II. Discontinuous conduction mode. IEEE Trans. Aerosp. Electron. Syst. 26(3), 497–505 (1990)
16. Migoni, G.A., et al.: A mixed modeling approach for efficient simulation of PWM switching mode power supplies. IEEE Trans. Power Electron. 34(10), 9758–9767 (2019)
17. Nabinejad, A., et al.: A systematic approach to extract state space averaged equations and small signal model of partial power converters. IEEE Journal of Emerging and Selected Topics in Power Electronics 8(3), 2475–2483 (2020)
18. Rajagopalan, J., et al.: A general technique for derivation of average current mode control laws for single-phase power-factor-correction circuits without input voltage sensing. IEEE Trans. Power Electron. 14(4), 663–672 (1999)
19. Choi, B., et al.: Modeling and small-signal analysis of controlled ontime boost power-factor-correction circuit. IEEE Trans. Indust. Electron 48(1), 136–142 (2001)
20. Alonso, J.M., et al.: A straightforward methodology to modeling high power factor ac–dc converters. IEEE Trans. Power Electron. 28(10), 4723–4731 (2013)
21. Fang, P., et al.: A multiplexing ripple cancellation led driver with true singlestage power conversion and flicker-free operation. IEEE Trans. Powe Electron. 34(10), 10105–10120 (2019)
22. Brown, R., Soldano, M.: One cycle control IC simplifies PFC designs. In: APEC 2005: Twentieth Annual IEEE Applied Power Electronics Conference and Exposition. IEEE, Austin, Texas 825–829 (2005)
23. Tiwari, S., et al.: Efficiency and conducted EMI evaluation of a singlephase power facto correction boost converter using state-of-the-art SiC MOSFET and SiC diode. IEEE Trans. Ind. Appl. 55(6), 7745–7756 (2019)
24. TDK Epcos - Metallized polypropylene film capacitors (MKP). https://www.tdk-electronics.tdk.com/inf/20/20/db/fc_2009/MKP_B32774_778.pdf. Accessed 31 July 2020
25. International Rectifier - IR1150(S)(PbF), IR1150I(S)(PbF) - µPFC one cycle control PFC IC. http://www.irf.ru/pdf/ir1150.pdf. Accessed 31 July 2020
26. Bamgboje, D.O., et al.: Low cost high performance LED driver based on a self-oscillating boost converter. IEEE Trans. Power Electron. 34(10), 10021–10034 (2019)
27. International Rectifier - Application Note AN-1077: PFC converter design with one-cycle control IC IR1150. https://www.infineon.com/dgdl/an-1077.pdf?fileId=5546d462533600a4015355 9563801007. Accessed 31 July 2020
28. Chu, C.-L., et al.: Improved one-cycle control for realizing ac/dc power factor correction boost converter. Sensors and Materials 31(7), 2213–2223 (2019)